Understanding the Population, Coordination, and Orientation of Water Species Contributing to the Nonlinear Optical Spectroscopy of the Vapor−Water Interface through Molecular Dynamics Simulations

Dave S. Walker, Dennis K. Hore, and Geraldine L. Richmond*

Department of Chemistry and Materials Science Institute, University of Oregon, Eugene, Oregon 97403

Received: May 18, 2006; In Final Form: July 12, 2006

Molecular dynamics simulations are used to deconvolve the vibrational spectral features of the vapor−water interface based on molecular environment. A simple geometric description of hydrogen bonding is deployed to identify the OH stretch modes that comprise the vibrational sum-frequency spectrum of the vapor−water interface with direct comparison to our experimental results. The population densities of different species of water molecules are presented as functions of interfacial depth and orientation. It is found that surface water molecules that possess one proton donor bond and one proton acceptor bond make the dominant contribution to both the SSP- and SPS-polarized spectral responses and are located within an angstrom of the Gibbs dividing surface.

Introduction

In recent years, much theoretical, computational, and experimental effort has been made to improve our understanding of interfacial water structure.[1−16] This interest is driven in part by the expanding application of vibrational sum-frequency spectroscopy (VSFS) to water surfaces.[4,9,10,13,14] As with other spectroscopic techniques, the complexity of the different types of hydrogen-bonding interactions between molecules at aqueous surfaces provides a challenge for spectral interpretation, as has been the case for interpreting the vibrational spectrum of water.

Computationally, frequency- and time-domain theories have been used to study the structure and dynamics of the water surface.[5−8] Time-domain approaches rely on a fewer number of empirical parameters and include dynamical effects observed in real systems that are unaccounted for in the frequency-domain approach.[16] Frequency-domain approaches, however, are generally more intuitive and are amenable to a normal-mode type of analysis that enables direct and simple correlation between an OH stretch mode and its vibrational frequency.

In this report, molecular dynamics simulations are used to provide a simple and intuitive description of the OH stretch region in a manner similar to that performed experimentally. A description of hydrogen bonding based on coordination is applied that allows for a system of water molecules to be categorized into different species. Density profiles are determined to describe how these species vary as a function of depth. Orientation distributions of OH bonds are measured to describe which species exhibit preferential alignment with respect to the water surface. The VSF spectrum of the vapor−water interface is then generated in two polarization schemes that probe OH bond alignment perpendicular (SSP) and parallel (SPS) to the surface. This computational approach allows for the deconvolution of VSF spectral features that goes beyond experimental interpretation and readily identifies spectral contributions from water species unobtainable by experimental methods.

* To whom correspondence should be addressed. E-mail: richmond@uoregon.edu. Telephone: 541-346-4635. Fax: 541-346-5859.

Computational Method

Simulations were performed on a box of POL3 water molecules using the AMBER 7 force field.[17] (Although a nonpolarizable water model was used in earlier studies,[9] polarizable water models have shown increased robustness when applied to water surfaces by allowing for the water dipole moment to vary as a function of proximity to the interface[18−20] and for the accurate solvation of ions at the interface.[21]) The initial box consisted of 2135 molecules and measured 40 Å in each direction to produce a bulk density of 0.997 g/mL. The bulk liquid was equilibrated for 200 ps before the periodic box was expanded by 40 Å in the *z* direction, producing an unoccupied volume of $(40\ \text{Å})^3$ and generating two interfacial systems with periodic boundaries applied in all three dimensions. (The water molecules from one interfacial system were related to those of the other by means of an inversion operation, allowing for constructive interference effects to accumulate between the two interfaces for parameters dependent upon molecular orientation.) After a 2 ns equilibration of the interfacial systems, configurations were recorded every 50 fs over the course of the following 3 ns. The time step of integration was 1 fs. The temperature was weakly coupled to a heat bath at 300 K to approximate the temperature with which the VSFS experiments described in this report were performed**.** The molecular geometries were constrained using the SHAKE algorithm, and the particle mesh Ewald technique applied an 8 Å cutoff to handle long-range interactions.

The recorded coordinate and force information was used to generate vibrational sum-frequency spectra according to the protocol developed by Morita and Hynes (MH).[5] They used ab initio methods to calculate gas-phase hyperpolarizability tensor elements for an uncoupled OH oscillator. The spring force model, expanded to include the first anharmonicity, used the force information extracted from MD simulations to calculate frequency shifts relative to the gas-phase frequencies of OH oscillators due to solvation of gas-phase water within the condensed-phase environment. The two OH oscillators were coupled to produce lower and higher energy states that converge

10.1021/jp063063y CCC: $33.50
Published on Web 08/24/2006

into symmetric and antisymmetric water modes when the oscillators are in similar environments. The molecular hyperpolarizability was then evaluated using

$$\beta_{pqr} \approx \frac{1}{2m\omega}\left(\frac{\partial\alpha_{pq}}{\partial Q}\right)\left(\frac{\partial\mu_r}{\partial Q}\right)\left[\frac{\omega-\omega_{IR}}{(\omega-\omega_{IR})^2+\gamma^2}+\frac{i\gamma}{(\omega-\omega_{IR})^2+\gamma^2}\right] \quad (1)$$

where the derivatives $\partial\mu_r/\partial Q$ and $\partial\alpha_{pq}/\partial Q$ are the infrared transition dipole moment and Raman transition polarizability derivatives, respectively, for an OH bond of reduced mass m and frequency ω in the pqr reference frame. The coordinate information was used to transform these derivatives from the molecular frame into the laboratory frame by means of Euler transformations. The physical interpretation of γ is often one of a phenomenological damping that is compared to the lifetime of the OH stretch; here it is simply treated as a convergence parameter.

In this study, a number of modifications have been made to the MH technique. First, a dipole−dipole interaction was implemented to model intermolecular coupling effects. This interaction is the standard classical electrodynamical solution and takes the form

$$V=\frac{1}{4\pi\epsilon_0 R^3}\left(\vec{\mu}_A\cdot\vec{\mu}_B-\frac{3(\vec{\mu}_A\cdot\vec{R})(\vec{R}\cdot\vec{\mu}_B)}{R^2}\right) \quad (2)$$

where μ_A and μ_B are dipole moment derivatives evaluated at the center of mass of the OH bond and R is the separation of OH oscillators from adjacent water molecules. This treatment was successful in the study of ice clusters[22] and has recently met success in the study of water.[3] This interaction was subject to the distance and angle restraints that describe hydrogen-bonding modes in this report (discussed below) by shifting the frequencies of affected OH stretch oscillators and enhancing the agreement between the computational and experimental spectra in the lower-frequency region of the spectrum.

Second, the intramolecular coupling constant was modified to accommodate for fully solvated water molecules. In the MH treatment, the coupling constant was set to half the separation between the gas-phase symmetric and antisymmetric stretching, $V_{12} = \Delta\nu_{12}/2 = 49.5\ \text{cm}^{-1}$, and was held fixed for all water molecules regardless of molecular environment. Studies of isotopic H_2O in D_2O have shown that the value of the coupling constant of water decreases to less than 25 cm^{-1} when those molecules are fully solvated.[23] On the basis of this observation, a simple perturbation to the coupling constant was applied:

$$V_{12}=\frac{49.5\ \text{cm}^{-1}}{\sqrt{N}} \qquad \text{for } N\neq 0 \quad (3)$$

where N is the number of hydrogen bonds on the molecule with at least one bond on a hydrogen atom. With this expression, gas-phase water retains its gas-phase value of the coupling constant, whereas solvated modes with four hydrogen bonds receive a value of 24.8 cm^{-1}. Fully solvated molecules generally do not possess large VSF responses, so their overall impact on the total VSF spectrum (especially in SSP polarization) is small. In the calculation of Raman and IR spectra, however (not shown), these solvated modes produce the greatest response and create structure in those spectra that are clearly artifact. Reducing the coupling constant to 30 cm^{-1} or less removed the false structural features and restored the overall line shape of those spectra.

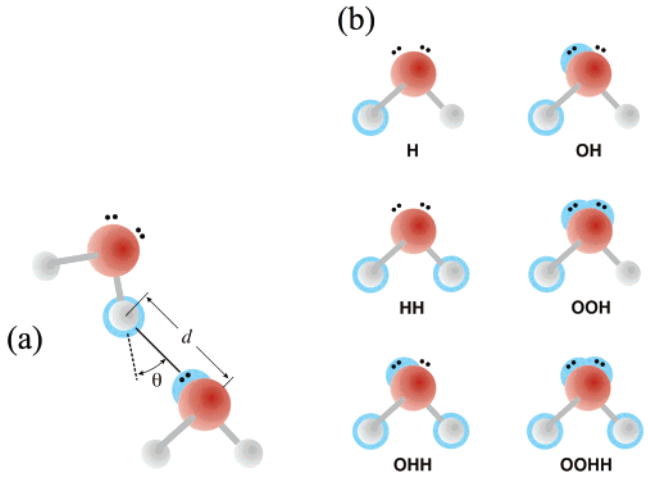

Figure 1. (a) Graphic showing hydrogen bond criterion of $d = 2.5$ Å and $\theta = 30°$. Bonds that satisfy both length and angle requirements are labeled as "normal" while those that only satisfy the length requirement are labeled as "broken". (b) Water molecules characterized by their hydrogen bonding to adjacent water molecules. The coordination labels represent the atoms in the water molecules that are involved in the bonding to adjacent water molecules.

Finally, a value of 2 cm^{-1} was used for the Lorentzian line width, γ. This is significantly smaller than the value of 22 cm^{-1} used by MH, but resulted in model VSF spectra that captured features of experimental vapor−water spectra unobtainable with the larger value.

Molecules were generally described as hydrogen bonded if their intermolecular OH separation was less than 2.5 Å and the angle between the intermolecular and intramolecular OH bond was less than 30°, as is shown in Figure 1a. (Molecules that satisfied these requirements were treated with the dipole−dipole interaction described earlier.) It was found, however, that these OH stretch modes alone did not reproduce the total intensity of the spectral results within the hydrogen-bonding region. While it is not uncommon to impose angle restraints on the description of an intermolecular OH bond,[24−26] studies have shown that imposing this restraint introduces the possibility of neglecting a substantial quantity of energetically favorable hydrogen bonds.[27] Because of this observation, intermolecular OH bonds were also identified if the angle requirement was not met, and these modes were distinguished from those that satisfied the angle requirement by labeling the latter as a "normal" hydrogen bond and the former as a "broken" hydrogen bond. The collection of both these types of bonds fully reproduced the total intensity of the OH stretch region.

In this report, the naming scheme used by Buch[3] is adapted, where hydrogen bonds located on the hydrogen atom that are typically described as "proton donors" are given the designation "H-bonded" species, while hydrogen bonds located on the oxygen atom that are typically described as "proton acceptors" are given the designation "O-bonded" species. Most of the different species of water molecules discussed using this scheme are shown in Figure 1b. Molecules that possess one proton donor bond and one proton acceptor bond are given the coordination label "OH-bonding", whereas those with tetrahedral bonding participate in "OOHH-bonding". In addition, molecules that possess purely "normal" hydrogen bonds by satisfying the length and angle restraints are given the prefix "*n*-" while those that possess "broken" hydrogen bonds by not satisfying the angle restraint are given the prefix "*b*-". With this notation, a water

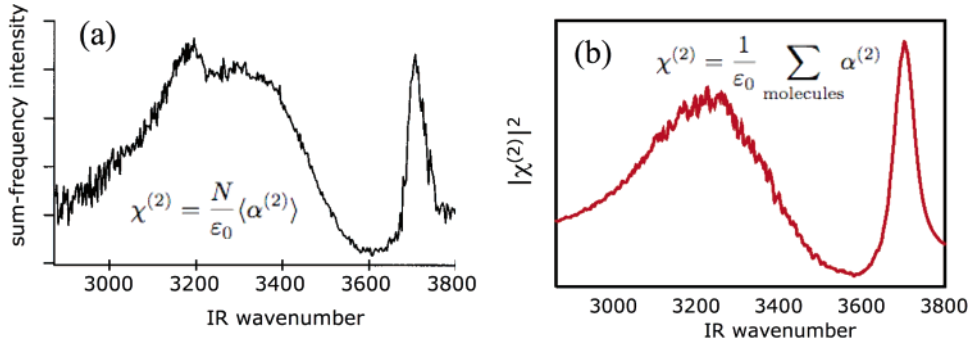

Figure 2. (a) Experimental and (b) computational SSP-polarized VSF spectra of the vapor−water interface. Spectra are corrected for local field effects and include the nonresonant contribution.

molecule that possesses one normal proton donor bond and one normal proton acceptor bond is identified as a "*n*-OH-bonded" molecule, while a molecule that possesses tetrahedral coordination where some or all of those bonds are "broken" is identified as a "*b*-OOHH-bonded" molecule. Molecules labeled without the "*n*-" or "*b*-" prefix represent contributions from the sum of the normal and broken species. Water molecules that do not possess any hydrogen bonds are commonly referred to as water "monomers" and will be labeled as such here. It should also be noted that only the four closest hydrogen bonds per molecule are considered for hydrogen-bonding characterization.

Water molecules with one OH oscillator hydrogen bonded through the hydrogen atom and the other OH oscillator not hydrogen bonded through the hydrogen atom have been described as possessing energetically "uncoupled" OH oscillators, which are identified separately in VSFS experiments as a "donor OH mode" and a "free OH mode", respectively.[28] Experimentally, they are described on a microscopic level as water molecules with the free OH oscillator pointing toward the vapor phase and the donor OH oscillator pointing toward the water. Because of experimental limitations, the degree to which these species are bonded to other water molecules through the oxygen atom is completely unknown for room-temperature experiments. In this computational work, the number of proton acceptor bonds per molecule is easy to identify, resulting in the generation of three different species of molecule that possess free and donor OH modes (H-, OH-, and OOH-bonded molecules). To aid the discussion, the naming scheme described above will be extended to these three modes by placing the coordination label before the free/donor OH mode designation, i.e., H-bonded free OH mode, *b*-OOH-bonded donor OH mode, or total free OH mode (which represents the sum of the H-, OH-, and OOH-bonded molecules that contains free OH oscillators).

Once the molecular hyperpolarizabilites were projected into the laboratory reference frame, they were binned according to frequency to create the complex macroscopic susceptibility, χ_{ijk}, which along with the nonresonant susceptibility was then squared to obtain the VSF spectrum:

$$I_{\text{SFG}} \propto |\chi_{ijk} + \chi_{\text{NR}}|^2 I_{\text{VIS}} I_{\text{IR}} \tag{4}$$

where χ_{NR}, the nonresonant susceptibility, can be determined using ab initio methods.[6] The local field correction (unit polarization vectors and Fresnel coefficients) needs to be accounted for when comparing computational results to direct experimental observations, but by correcting experimental spectra for this effect, it need not be included for computational comparison.

The experimental and computational VSF spectra of the vapor−water interface in SSP polarization are shown in Figure 2. The semiempirical magnitude of the nonresonant susceptibility used in the computational spectrum is a real, negative constant chosen to reproduce the experimental line shape, and both spectra have been corrected for local field effects. With the exception of the small experimental feature at 3200 cm^{-1} and the narrow experimental peak at 3700 cm^{-1}, the computational agreement with experiment is very good.[9] The small experimental feature at 3200 cm^{-1} is a combination of noise and signal and is questionable in its reproducibility, and so the computational correction for this feature is not currently being pursued rigorously. While it has been shown that the motional averaging for a given OH stretch mode can account for the line shape narrowing observed experimentally,[3,27] no attempt has been made to include it in this work in order to alleviate the issue of characterizing an OH oscillator that changes its identity during the course of this averaging. It should be noted that the motional narrowing effect is not related to the value of the Lorentzian width used in the frequency-domain approach, but the value of the Lorentzian width can "disguise" the degree to which this effect is neglected in the spectral response.[8] A more accurate treatment of this effect would involve averaging within the calculation of frequencies prior to applying the broadening term represented by the Lorentzian width. Consequentially, while most peak frequencies described for a given OH stretch mode are not affected, their "line widths" will be broader in appearance compared to the expected line widths extracted from experiment and is most apparent in the peak that occurs at 3700 cm^{-1}.

Results and Discussion

Density Profiles. The number of water molecules within the periodic box was configured to achieve a bulk density of 0.997 g/mL. The fractional values of the different OH species approximately represent percentages of total density. Figure 3a shows the density profiles of the major populations of water species as a function of the *z*-coordinate. The horizontal axis represents the *z*-coordinate, where values of $z < 0$ Å represent the water region, values of $z > 0$ Å represent the vapor region, and $z = 0$ Å approximates the Gibbs dividing surface. The OHH-bonded and OOHH-bonded water molecules follow the total water density profile, with their maximum densities in the bulk and decreasing in concentration as they cross the dividing surface. In contrast, the densities of H-, OH-, and OOH-bonded molecules are low within the bulk and increase as they approach the dividing surface. The total free density profile that represents the sum of these molecules peaks in population at approximately 0.25 g/mL, within reasonable agreement with experimental estimates.[11,14] In addition, near the Gibbs dividing surface, these

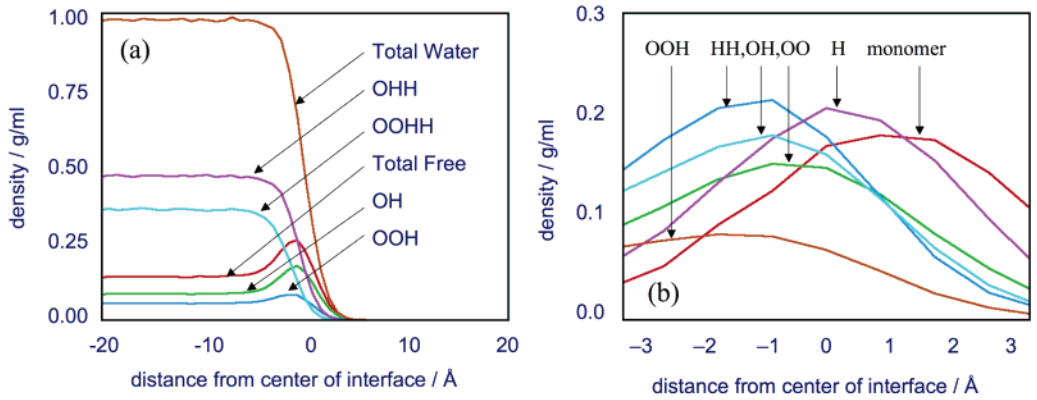

Figure 3. (a) Density profiles of major water species. The water region is located at $z < 0$ Å, the vapor region is located at $z > 0$ Å, and the Gibbs dividing surface is located approximately at $z = 0$ Å. From largest to smallest: orange, total water; purple, OHH-bonded water; light blue, OOHH-bonded water; red, all molecules containing a free OH bond; green, OH-bonded water; blue, OOH-bonded water. (b) Profiles of water species that possess peak densities at the interface. From left to right: orange, OOH-bonded water; blue, HH-bonded water (×100); light blue, OH-bonded water; green, OO-bonded water (×10); purple, H-bonded water (×50); red, water monomers (×200).

molecules have a greater population than those of both OHH- and OOHH-bonded molecules and comprise a significant portion of the remaining water density surrounding the dividing surface. These surface concentrations are also in good general agreement with the computational characterization of the water surface at room temperature using the EMP polarizable model recently deployed by Buch.[3] The notable difference arises from the surface populations of three-coordinated water molecules; in this work, OHH and OOH molecules are larger and smaller in surface populations, respectively, a difference that is most likely due to the different computational models and descriptions of hydrogen bonding.

When distinguishing between normal and broken bonding configurations for H-, OH-, and OOH-bonded water molecules, *n*-OH-bonded molecules comprise the largest percentage and have a peak population of about 0.14 g/mL (51%), followed by *b*-OOH-bonded molecules (22%), *b*-OH-bonded molecules (15%), and *n*-OOH-bonded molecules (11%). H-bonded molecules only comprise 1% of all donor molecules and are not broken down into "*n*-" or "*b*-" species due to their low density. These results suggest that the oxygen atom of these water molecules is readily available for a "normal" hydrogen bond (as is indicated by the most dominant species of donor molecule, *n*-OH-bonded molecules) but is less likely to form a third bond, as shown by the lower density of *b*-OOH-bonded molecules in the interfacial region.

OHH- and OOHH-bonded molecules do not possess peak concentrations at the interface. Of these species, the profile of *n*-OHH-bonded molecules has a density of approximately 0.3 g/mL while the profile of *n*-OOHH-bonded molecules has a density of only 0.15 g/mL. Moving from the water region toward the vapor region across the Gibbs dividing surface, *n*-OHH-bonded molecules are second in population only to water molecules that possess free and donor OH oscillators, while the profile of *n*-OOHH-bonded molecules is small in population and decreases throughout the interfacial region.

Other low-population species (monomer, HH-, OO-, and O-bonded species, where the sum of OO- and O-bonded species will be labeled only as OO henceforth) that are difficult to identify experimentally are readily identifiable in these calculations. Of these species, only the profile of OO-bonded molecules exceeds 0.01 g/mL in peak population.

The vapor−water interfacial region is generally measured to be a few molecular layers thick, or about 6 Å.[9] Figure 3b shows a more detailed density profile of water species that peak at the interface within these few molecular layers. The profiles of monomer, H-, OO-, and HH-bonded molecules have been scaled in order to fit the graph. The ordering of the peak locations indicate that molecules with a larger quantity of hydrogen bonds reside deeper within the water region, and those molecules with a smaller quantity of hydrogen bonds reside closer toward the vapor region. These results agree with our experimental observation in that they show interfacial water molecules with greater degrees of coordination are more immersed within the water phase compared to those with smaller degrees of coordination.[29,30]

Orientation Distributions. Figure 4a shows a schematic representing tilt angles of the individual OH bonds for a water molecule at the interface. With the positive *z*-axis pointing into the vapor region, the angle range $0 < \theta < \pi/2$ will be described as being "above" the plane of the interface (the vapor region), while the angle range $\pi/2 < \theta < \pi$ will be described as being "below" the plane of the interface (the water region). Only those molecules that possess net orientations will contribute to VSF intensity for a given polarization. With knowledge of the number densities and orientation distributions of the individual OH bonds, VSF intensities from these molecules can be determined. Although five vectors were applied to describe the orientation distributions of water (two OH bond vectors, an HH bond vector, the C_{2V} axis vector, and the vector normal to the molecular plane), only the OH bond vectors will be discussed in this report. Orientation profiles are normalized by sin θ, which causes the OH bond vector distributions to appear as flat functions of tilt angle for isotropic averages. The tilt angle distributions of OH bond vectors are measured independently, and the orientation preference of one OH bond cannot be immediately correlated to that of the other bond (as a result of tracking only OH bond vectors). However, some general observations can be made, with immediate implications to the spectral contributions in VSFS.

Only the orientation distributions of water molecules that possess free and donor OH bonds show net tilt angle differences between their two OH bonds. As is shown in Figure 4b, the orientation distribution of the total free OH bond (from H-, OH-, and OOH-bonded species) shows overall preference above the plane, while that of the total donor OH bond shows overall preference below the plane. Of these different bonded species, the donor and free OH modes from OH-bonded molecules show the strongest orientation features. Figure 4c shows that the orientation distribution of the free OH bond and the corresponding donor OH bond from OH-bonded molecules follow the trend

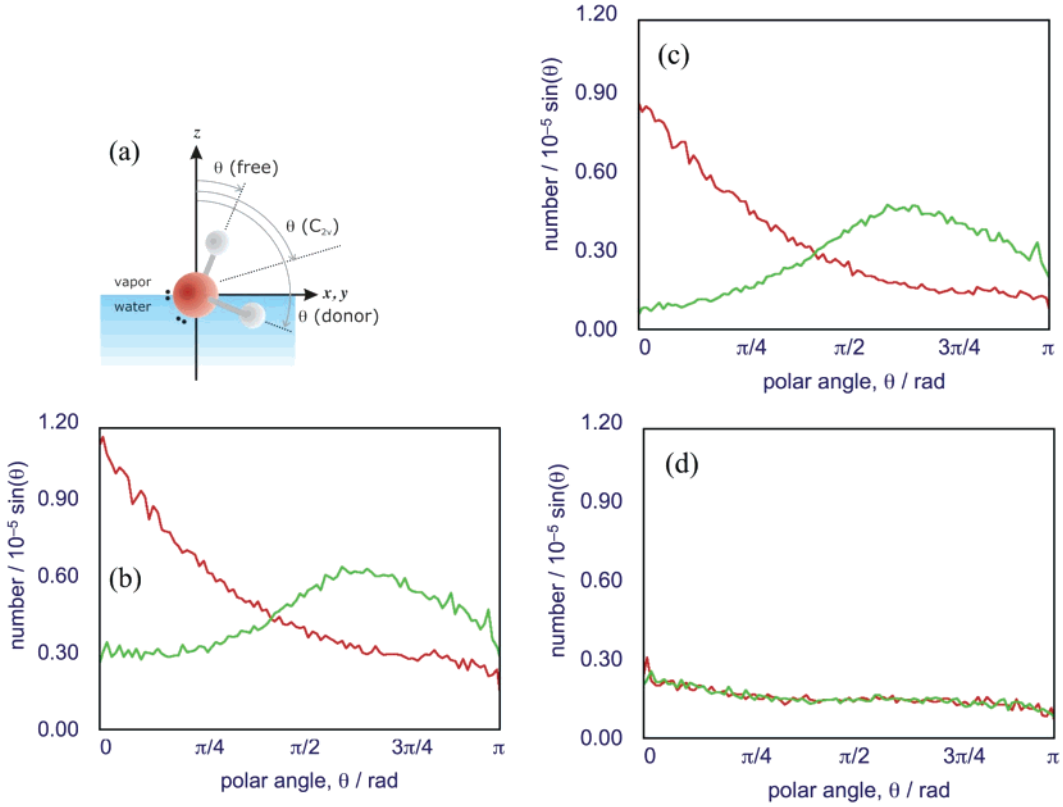

Figure 4. (a) Graphic showing tilt angles for the OH bonds of water. The *z* axis points from the water surface toward the vapor. Orientation distributions of: (b) all free OH bonds (red) and all donor OH bonds (green); (c) OH-bonded free OH bonds (red) and donor OH bonds (green); (d) OOH-bonded free OH bonds (red) and donor OH bonds (green). In each case, 30 Å of bulk water is excluded.

observed in Figure 4b. In contrast, Figure 4d shows that the orientation distribution of the next highest density species, OOH-bonded molecules, possess free OH and donor OH bonds that are relatively flat and overlay each other throughout the entire angle range. The predictable consequence of this broad tilt angle distribution for OOH-bonded molecules compared to that of OH-bonded molecules is a smaller SSP-polarized VSF response from OOH-bonded molecules compared to OH-bonded molecules.

Among all donor species, the orientation distribution of the H-bonded donor OH bond (not shown) exhibits the steepest angle preference below the plane; however, the VSF response for this molecule is hindered by extremely low population density compared to that of other donor species. The orientation distributions of water monomers (not shown) also exhibits a small tilt angle preference below the plane, but is also hindered by extremely low population density. (On the basis of the hydrogen-bonding criterion applied in this work, water molecules only need to be 2.5 Å away from other molecules to be considered as monomers, at which length external forces will still be nonzero.) The orientation distribution of OO-bonded molecules (not shown) exhibits a tilt angle preference above the plane, with a broad distribution similar to that of OOH-bonded molecules. From these observations, it appears unlikely that VSF responses from H-bonded molecules or water monomers will be observable, but with a sensitive enough experimental probe, it appears quite possible to observe a VSF response from OO-bonded molecules, as these molecules do possess quantitative number densities and orientation preferences. To date, OO-bonded water molecules have not been observed with VSFS for the vapor−water interface but have been proposed for the CCl_4−water interface[31] and in X-ray scattering studies of water by the Saykally group.[32]

Of the water species that do not possess peak densities at the interface, orientation distributions of OHH-bonded molecules peak slightly below the surface, while those of OOHH-bonded molecules peak about parallel to the surface. Combining these observations with their respective number densities, OHH-bonded molecules are likely to contribute more VSFS response than OOHH-bonded molecules in SSP polarization, and both species are likely to produce significant VSFS responses in SPS polarization. This will be discussed in more detail later.

SSP-Polarized Sum-Frequency Spectral Response. The VSF response of the system brings the OH stretch populations and orientation profiles together with their transition strengths to produce a spectrum that is selective of the water surface. To characterize the OH stretch modes, a VSF spectrum that contains a nonresonant susceptibility and/or local field effects must correct for these in order to accurately assess the resonant response from those OH stretch modes. (Figure 2 shows experimental and computational examples of VSF spectra that contain a nonresonant susceptibility but have local field effects removed.) The computational, SSP-polarized VSF spectrum for the vapor−water interface that has been corrected for both the nonresonant susceptibility and local field effects is shown in Figure 5a.

By far the most dominant feature is that of the total free OH mode, which peaks at 3693 cm^{-1}. The *n*-OH-bonded donor OH stretch mode shows a very strong presence and dominates the hydrogen-bonded region, displaying a larger intensity than all other OH stretch modes combined. This is consistent with its large population density and also its strong orientation preference. The large presence of the molecules contributing to the free OH mode (predominately *n*-OH-bonded molecules) and the donor OH mode (also predominately *n*-OH-bonded donor species) shows the spectral contribution in SSP polarization

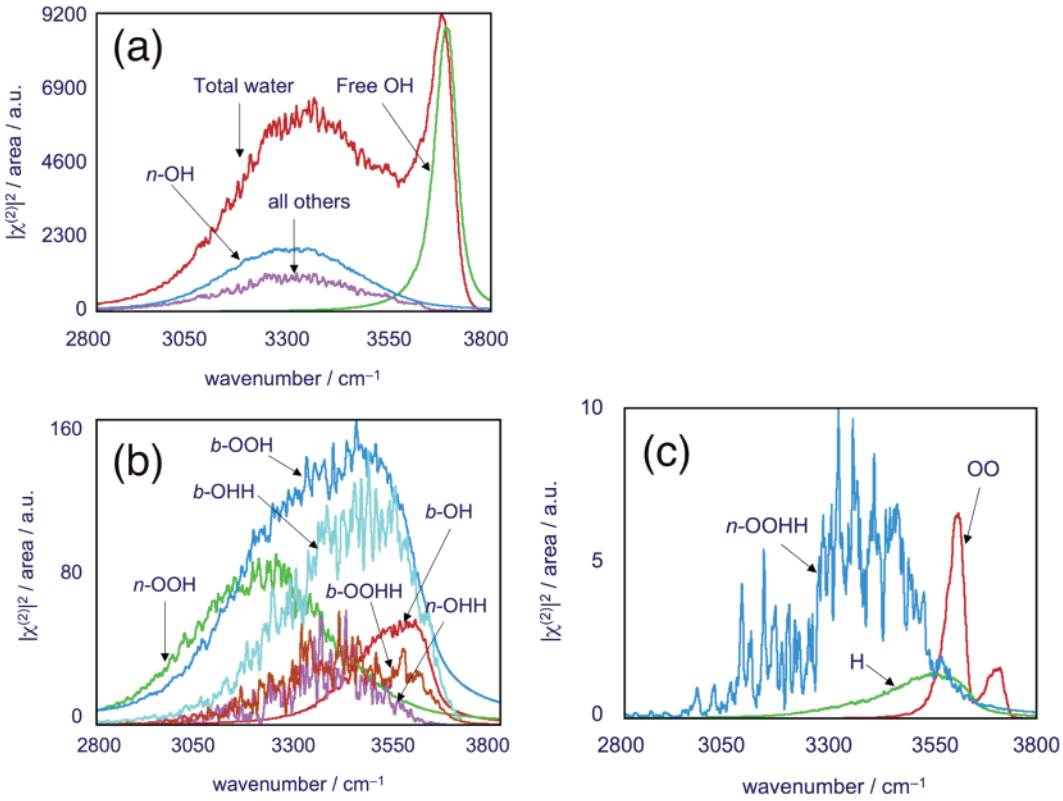

Figure 5. (a) Resonant SSP-polarized vapor−water spectrum with contributions from the most intense OH stretch modes. Red, total spectrum; green, sum of all free OH modes; blue, donor OH modes with *n*-OH-bonding; purple, all other modes combined; (b) spectral contributions to the vapor−water spectrum from the next most intense OH stretch modes. From largest to smallest: blue, *b*-OOH-bonded water molecules; light blue, *b*-OHH-bonded water molecules; green, *n*-OOH-bonded water molecules; red, *b*-OH-bonded water molecules; orange, *b*-OOHH-bonded water molecules; purple, *n*-OHH-bonded water molecules; (c) spectral contributions from OH stretch modes of low intensity. Blue, *n*-OOHH-bonded water molecules; red, OO-bonded water molecules; green, H-bonded water molecules.

comes primarily from water molecules with one "normal" proton acceptor bond and one "normal" proton donor bond.

Figure 5b shows spectral contributions to the SSP-polarized spectrum from the next largest set of OH stretch modes. Although these individual spectral contributions are small compared to that of the *n*-OH-bonded donor OH mode, their collective contribution is significant, as is shown in Figure 5a. The *b*-OOH-bonded donor OH mode is the largest contributor in this set, followed by those of OHH- and OOHH-bonded molecules. Of the OHH- and OOHH-bonded molecules, the spectral contributions from *n*-OHH, *b*-OHH, and *b*-OOHH-bonded molecules are of comparable intensity. Figure 5c shows the spectral contributions of low intensity OH stretch modes. Included here are the spectral responses from *n*-OOHH-, H-, and OO-bonded molecules. The orientation distribution of OO-bonded molecules indicates this type of molecule points both its hydrogen atoms toward the vapor phase, and by description, neither hydrogen atom is impacted by hydrogen-bonding effects. As a result, the OH bonds of OO-bonded molecules are in similar environments producing clear symmetric and antisymmetric stretches. The symmetric stretch mode oscillates approximately perpendicular to the interface, resulting in preferential detection over the antisymmetric stretch in SSP polarization.

On the basis of the description of hydrogen bonding and intermolecular coupling provided in this report, some general remarks can be made. "Normal" OH stretch modes have peak intensities between 3200 cm^{-1} and 3400 cm^{-1}, while "broken" OH stretch modes tend to peak above 3400 cm^{-1}. With the exception of the total free OH, monomer, and OO-bonded OH stretch modes, these peaks are broad, spanning hundreds of wavenumbers and containing large degrees of overlap. Many of these peaks are clearly asymmetric in their line shape. Water molecules that possess only one or two hydrogen bonds have higher peak frequencies compared to those molecules that possess higher degrees of coordination, but for all cases of hydrogen-bonded modes, the peak frequency appears to be more dependent on the strength of the hydrogen bonds than it is on the number of hydrogen bonds.

While the determination of the total free OH stretch mode is generally accepted, the spectral deconvolution of the hydrogen-bonding region continues to be a subject of debate, in particular the location of the donor OH mode. Different experimental approaches have been used to obtain somewhat simplistic spectral assignments as an important first step toward understanding the complex nature of hydrogen bonding at a water surface. These calculations demonstrate the necessity to move to the next level of sophistication in the spectral interpretation of the OH stretch region of neat water with different degrees of bonding interactions, interfacial depth, and surface orientation. For example, these calculations show that the dominant donor OH stretch mode (the *n*-OH-bonded donor OH mode) contributes spectral intensity broadly across the entire hydrogen-bonded region rather than specific regions suggested by other studies.[4,9,13] It is interesting to note that these results also indicate that other bonded modes (the *b*-OOH-bonded donor OH mode, the *n*-OOH-bonded donor OH mode, etc.) are fairly localized in distinct spectral regions.

What is clear from these calculations and those of Buch[3] is that development of a deeper understanding of the OH stretch modes contributing to the VSF spectrum requires, as a first step, a simpler hydrogen-bonding system. An ideal case is afforded

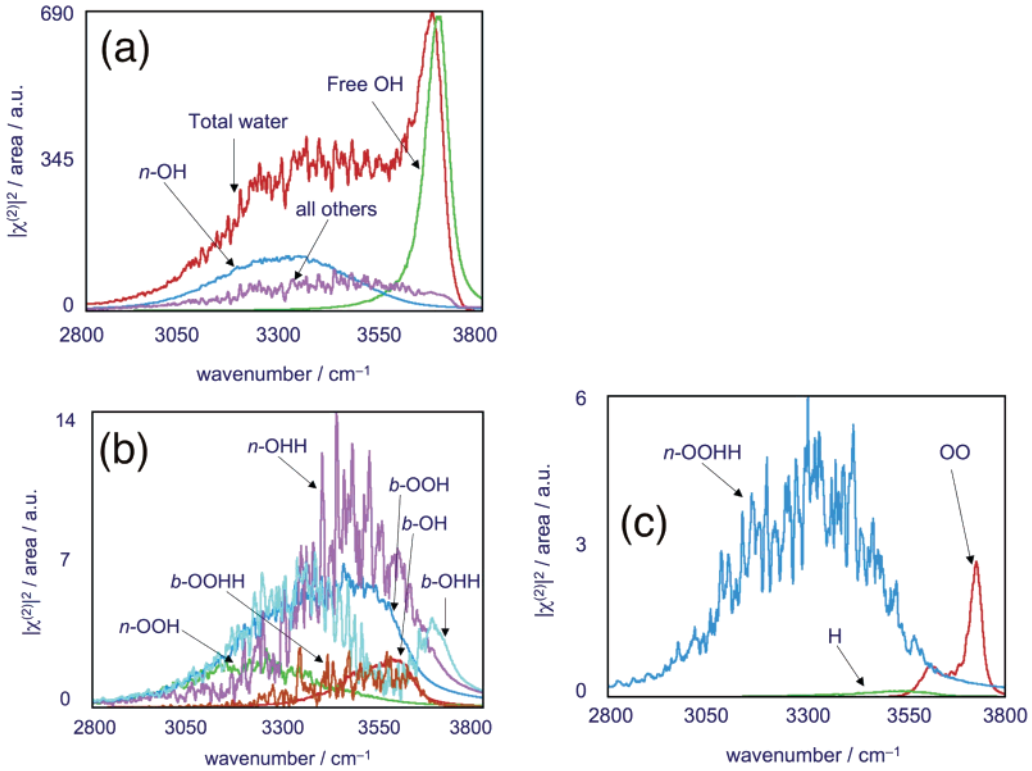

Figure 6. (a) Resonant SPS-polarized vapor−water spectrum with contributions from the most intense OH stretch modes. Red, total spectrum; green, all free OH modes; blue, donor OH modes with *n*-OH-bonding to two adjacent water molecules; purple, all other modes combined; (b) spectral contributions from the next most intense OH stretch modes. From largest to smallest: purple, *n*-OHH-bonded species; light blue, *b*-OHH-bonded species; blue, *b*-OOH-bonded species; green, n-OOH-bonded species; red, *b*-OH-bonded species; orange, *b*-OOHH-bonded species; (c) spectral contributions from OH stretch modes of low intensity. Blue, *n*-OOHH-bonded species; red, OO-bonded species; green, H-bonded species.

by isotopic dilution experiments that measure the VSF spectrum of surface HOD in D_2O.[9] Such experiments greatly reduce the complications of intermolecular and intramolecular coupling known to cause broadening of affected OH stretch modes. For this system, preliminary simulations of the VSF response from HOD/D_2O surfaces[33] show the frequency of the uncoupled solvated donor OH stretch mode converging to 3450 cm^{-1}, corresponding well with experimental observations. The calculations reported here indicate that, in the case of pure H_2O, this uncoupled donor OH mode broadens and consists of *n*-OH-bonded donor OH modes with additional contributions from *b*-OOH-bonded donor OH modes. Other contributors are also present in the spectral assignments of the donor OH mode carefully made by other groups. Liu et al.,[4] who applied curve-fitting routines using VSF spectra of the vapor−water interface and ATR−IR and Raman studies of bulk water, have assigned the donor OH mode to an OOH-bonded species occurring at 3250 cm^{-1}. These calculations indicate (see Figure 5b) that an *n*-OOH-bonded donor OH mode does indeed contribute to this spectral region. However, the 3250 cm^{-1} assignment misses the contributions of donor OH modes that are present with less constrained bonding (such as the *b*-OH-bonded and *n*-OH-bonded donor OH modes) that reside at the topmost surface layer, possibly a result of the reliance on the less surface sensitive ATR−IR and Raman studies used to assist in the spectral deconvolution. Gan et al.[13] used polarization analysis to conclude that a single-bonded donor OH mode (the H-bonded donor OH mode) must lie at higher frequencies (3550 cm^{-1}). These calculations (see Figure 5c) and the work of Buch[3] indicate that the H-bonded donor OH mode does contribute to that spectral region but that it is extremely low in population. This assignment misses the major donor OH modes that are shown here to be important contributors.

It is interesting to note a comparison with theoretical contributions to this issue, where Perry et al.[8] applied a time-domain approach to identify one of three peaks at 3325 cm^{-1}, coinciding well with the *n*-OH-bonded donor OH mode observed in this work (3310 cm^{-1}). The two other peaks were located within the low (3195 cm^{-1}) and middle (3400 cm^{-1}) portions of the hydrogen-bonding region.

Low-population OH stretch modes that are difficult to identify experimentally are identified in this study. OH stretch frequencies from OO-bonded molecules (see Figure 5c) appear at 3607 and 3701 cm^{-1}, while those of the water monomer (not shown) appear at 3631 and 3726 cm^{-1}, respectively. The frequency of the total free OH mode is slightly lower than that observed in experiments,[9] and those of the water monomer are slightly lower than the gas-phase values (3657 and 3756 cm^{-1}). These frequencies are not impacted by dipole−dipole interactions, and their intramolecular coupling constants are either gas-phase (water monomers and OO-bonded molecules) or largely unaffected by solvation (total free OH stretch mode). Therefore, these OH stretch modes are the easiest modes to compare to experimental values, and the systematically small discrepancies serve as a simple indication of the degree of accuracy of the computational approach used in this study.

SPS-Polarized Sum-Frequency Spectral Response. The resonant computational spectrum in SPS polarization was collected and is shown in Figure 6a. Direct comparison between the computational SPS-polarized spectrum and the experimental SPS-polarized spectrum is currently difficult because of challenges in determining a value for the nonresonant susceptibility that is consistent between computation and experiment. It is suspected that the total free OH peak determined computationally is larger relative to the hydrogen-bonding region than that obtained experimentally, due in part to this nonresonant term.

Nevertheless, some insights can be obtained about contributions to the SPS-polarized VSF spectrum from the calculations.

Compared to SSP polarization, there is significantly more intensity observed experimentally between the peak describing the total free OH mode and the peak describing the hydrogen-bonding region. Furthermore, within this higher-wavelength region, the spectral contribution from the *n*-OH-bonded donor mode no longer dominates over the collective contributions from the other hydrogen-bonded molecules. Figure 6b shows contributions to the SPS-polarized VSF spectrum from the next largest set of OH stretch modes and provides some insight as to how the spectral contributions differ between SSP and SPS polarization. Compared to SSP polarization (see Figure 5b), spectral responses from OHH-bonded molecules are larger in SPS polarization relative to contributions from other molecules of comparable magnitude. While the spectral response from *b*-OOHH-bonded molecules still appears small in SPS polarization, its intensity is approximately equal to that of the *n*-OOH-bonded donor OH stretch mode, whereas in SSP polarization, the *n*-OOH-bonded donor OH stretch mode was twice as large. Figure 6c shows the spectral response from *n*-OOHH-bonded molecules in SPS polarization is almost as intense as it is in SSP polarization. In addition, the antisymmetric stretch from OO-bonded molecules is preferentially probed over the symmetric stretch due to its orientation, roughly parallel to the interface. These results are consistent with the general assignment of the VSF intensity in the SPS spectra to "in-plane" bonded species made in the studies of Tarbuck and Richmond.[30]

Generally, the SPS-polarized spectrum is approximately a factor of 10 smaller than the SSP-polarized spectrum, and most of the corresponding OH stretch modes follow this trend in intensity. The spectral responses from *n*-OHH- and *n*-OOHH-bonded molecules, however, are only reduced by about a factor of 2 or less, making their spectral intensities larger in SPS polarization relative to other OH stretch modes than those in SSP polarization. OH stretch modes from OHH- and OOHH-bonded molecules are sometimes referred to as "in-plane" modes, and with orientation distributions that lie approximately parallel to the surface, it is reasonable that their contributions will be more significant in SPS polarization than those in SSP polarization.

Summary and Conclusions

Density profiles and orientation distributions are combined with molecular transition strengths to compute a VSF spectrum for water in SSP and SPS polarizations, which are then deconvolved to provide a detailed description of the different bonded species contributing to the OH stretch region of water. Density profiles show that water molecules with higher coordination are more immersed within the water phase compared to those with lower coordination. Orientation profiles show that interfacial molecules that possess both a free OH and donor OH bond (those that have been referred to as molecules that straddle or bridge the interface) show uniquely different tilt angle distributions between their OH bonds. This is particularly true for those molecules with OH-bonding but not for those with OOH-bonding. On the basis of these observations, the dominant spectral contribution to both SSP- and SPS-polarized VSF responses can be clearly attributed to water molecules that possess one "normal" proton acceptor bond and one "normal" proton donor bond. These particular molecules primarily reside within an angstrom of the Gibbs dividing surface.

The molecular scale knowledge obtained from this computational approach allows for a detailed spectral deconvolution of the OH stretch region. This level of detail is unobtainable experimentally, but is validated by the consistency of the macroscopic spectral result with respect to experiment. The computational approach also allows for another means of comparing OH stretch modes that are routinely identified experimentally via curve-fitting routines and are restricted to more simplistic spectral assignments and discussion. The description of the vapor−water interface that emerges from these calculations shows a multitude of interactions that vary in a consistent manner as a function of interfacial depth and is in good agreement with several general characteristics derived from the experimental studies from this laboratory.[9,30] Both experiment and computation indicate that the topmost interfacial layer is composed of water molecules with low degrees of coordination to adjacent water molecules. These species are found within the higher-frequency region of the VSF spectrum. It is found in both cases that those molecules with stronger intermolecular coupling reside somewhat deeper in the interfacial region and appear in the lower-frequency region. Both approaches also indicate that the most dominant contributors to the SSP spectrum are the highly oriented free OH and donor OH mode, largely due to high population and orientation.

In comparing calculated spectral features with those obtained experimentally, OH stretch modes unaffected by intermolecular coupling and largely unaffected by the value of the intramolecular coupling constant reveal that this computational approach agrees reasonably well with experimental results. To test the robustness of the description of hydrogen bonding, the dipole−dipole interaction used to describe intermolecular coupling and the simple expression for the solvation-dependent intramolecular coupling constant applied here, additional systems need to be studied. One test for this or any model is to apply the different methods to the isotopic dilution data obtained from VSF studies of H_2O-D_2O solutions,[9] a direction currently pursued by this laboratory. Additional applications of this approach will be geared toward liquid−liquid systems of varying polarity, experiments that have also been performed by this laboratory.[12]

Acknowledgment. We thank the National Science Foundation (CHE 0243856) and the Department of Energy, Basic Energy Sciences (DEFG02-96ER4557) for supporting this study. We also value enlightening discussions with Prof. Victoria Buch on coupling effects in water.

References and Notes

(1) Benjamin, I. *Phys. Rev. Lett.* **1994**, *73*, 2083.
(2) Brown, M. G.; Walker, D. S.; Raymond, E. A.; Richmond, G. L. *J. Phys. Chem. B* **2003**, *107*, 237.
(3) Buch, V. *J. Phys. Chem. B* **2005**, *109*, 17771.
(4) Liu, D.; Ma, G.; Levering, L. M.; Allen, H. *J. Phys. Chem. B* **2004**, *108*, 2252.
(5) Morita, A.; Hynes, J. T. *Chem. Phys.* **2000**, *258*, 371.
(6) Morita, A.; Hynes, J. T. *J. Phys. Chem. B* **2002**, *106*, 673.
(7) Perry, A.; Ahlborn, H.; Space, B. *J. Chem. Phys.* **2003**, *118*, 8411.
(8) Perry, A.; Ridley, C.; Space, B. *Chem. Rev.* **2006**, *106*, 1234.
(9) Raymond, E. A.; Tarbuck, T. L.; Brown, M. G.; Richmond, G. L. *J. Phys. Chem. B* **2003**, *107*, 546.
(10) Shultz, M. J.; Baldelli, S.; Schnitzer, C.; Simonelli, D. *J. Phys. Chem. B* **2002**, *106*, 5313.
(11) Superfine, R.; Du, Q.; Freysz, E.; Shen, Y. R. *Phys. Rev. Lett.* **1993**, *70*, 2313.
(12) Walker, D. S.; Brown, M. G.; McFearin, C. L.; Richmond, G. L. *J. Phys. Chem. B* **2004**, *108*, 2111.
(13) Gan, W.; Wu, D.; Zhang, Z.; Feng, R.; Wang, H. F. *J. Chem. Phys.* **2006**, *124*, 114705.
(14) Shen, Y. R.; Ostroverkhov, V. *Chem. Rev.* **2006**, *106*, 1140.
(15) Mucha, M.; Frigato, T.; Levering, L. M.; Allen, H.; Tobias, D. J.; Dang, L. X.; Jungwirth, P. *J. Phys. Chem. B* **2005**, *109*, 7617.

(16) Morita, A. *J. Phys. Chem. B* **2006**, *110*, 3158.
(17) Case, D. A.; Pearlman, D. A.; Caldwell, J. W.; Cheatham, T. E., III; Wang, J.; Ross, W. S.; Simmerling, C. L.; Darden, T. A.; Merz, K. M.; Stanton, R. V.; Cheng, A. L.; Vincent, J. J.; Crowley, M.; Tsui, V.; Gohlke, H.; Radmer, R. J.; Duan, Y.; Pitera, J.; Massova, I.; Seibel, G. L.; Singh, U. C.; Weiner, P. K.; Kollman, P. A. *AMBER 7*; University of California, San Francisco: San Francisco, 2002.
(18) Dang, L. X.; Chang, T. M. *J. Chem. Phys.* **1997**, *106*, 8149.
(19) Dang, L. X. *J. Phys. Chem. B* **2001**, *105*, 804.
(20) Kuo, W.; Mundy, C. J.; Eggimann, B. L.; McGrath, M. J.; Siepmann, J. I.; Chen, B.; Vieceli, J.; Tobias, D. J. *J. Phys. Chem. B* **2006**, *110*, 3738.
(21) Jungwirth, P.; Tobias, D. J. *J. Phys. Chem. B* **2001**, *105*, 10468.
(22) Buch, V.; Devlin, J. P. *J. Chem. Phys.* **1999**, *110*, 3437.
(23) Sadlej, J.; Buch, V.; Kazimirski, J. K.; Buck, U. *J. Phys. Chem. A* **1999**, *103*, 4933.
(24) Wernet, P.; Nordlund, D.; Bergmann, U.; Cavalleri, M.; Odelius, M.; Ogasawara, H.; Naslund, L. A.; Hirsch, T. K.; Ojamae, L.; Glatzel, P.; Pettersson, L. G. M.; Nilsson, A. *Science* **2004**, *304*, 995.
(25) Luzar, A.; Chandler, D. *Phys. Rev. Lett.* **1996**, *76*, 928.
(26) Lawrence, C. P.; Skinner, J. L. *Chem. Phys. Lett.* **2003**, *369*, 472.
(27) Moller, K. B.; Rey, R.; Hynes, J. T. *J. Phys. Chem. A* **2004**, *108*, 1275.
(28) Raymond, E. A.; Tarbuck, T. L.; Richmond, G. L. *J. Phys. Chem. B* **2002**, *106*, 2817.
(29) Richmond, G. L. *Chem. Rev.* **2002**, *102*, 2693.
(30) Tarbuck, T. L.; Richmond, G. L. *J. Am. Chem. Soc.* **2006**, *128*, 3256.
(31) Scatena, L. F.; Richmond, G. L. *J. Phys. Chem. B* **2001**, *105*, 11240.
(32) Wilson, K. R.; Cavalleri, M.; Rude, B. S.; Schaller, R. D.; Nilsson, A.; Pettersson, L. G. M.; Goldman, N.; Catalano, T.; Bozek, J. D.; Saykally, R. J. *J. Phys.: Condens. Matter* **2002**, *12*, L221.
(33) Walker, D. S.; Richmond, G. L. To be published.